Materials Research. 2024; 27(suppl. 1):e20230541
DOI: https://doi.org/10.1590/1980-5373-MR-2023-0541

Sigma Phase Detection in Duplex Stainless Steel Based on Correlation to Current and Potential in Micro Electrode Electrochemical of Surface

Elan Gabriel Forteski[a]*, Rodrigo Helleis[a], Renata Bachmann Guimarães Valt[a],

Leonardo Henrique Gomes[a], Jorge Omar Rios[a], Carolina Mocelin Gomes Pires[a],

Haroldo de Araújo Ponte[a], Maria José Jerônimo de Santana Ponte[a]

[a] Universidade Federal do Paraná, Programa de Pós-Graduação em Engenharia Mecânica, Curitiba, PR, Brasil.

Received: December 11, 2023; Revised: April 01, 2024; Accepted: April 02, 2024

Duplex stainless steels are widely used due to their good mechanical properties and corrosion resistance. However, they are susceptible to microstructural fragility related to harmful transformations taking place in intermetallic phases, such as the sigma phase. These transformations reduce mechanical properties like toughness and corrosion resistance. The current study aims to analyze the effect of different thermodynamic- and electrochemical-reactive phases based on using both linear sweep voltammetry tests as non-destructive tests, as well as the concept of microelectrodes. This technique is capable of detecting small amounts of intermetallic phases at the UNS-S31803 duplex stainless steel surface. Results have evidenced the influence of reduced electrode-solution exposure area on improving sensitivity for deleterious phase analyses. Peak potential and current peak recorded direct correlation to sigma phase concentration and it enabled detecting very low sigma-phase surface concentration, at the order of 0.04%. The study has shown improved sensitivity of linear sweep voltammetry tests used to detect harmful phases in duplex stainless steels.

Keywords*: Reactive micro-area, electrochemical sensitivity, deleterious phase, Non-destructive Test.*

1. Introduction

Alloys forming duplex stainless steels (DSS) can be developed based on different compositions to find different microstructural arrangements and to provide the material with better properties. In some cases, steels undergo thermomechanical processes[1]. DSS are steels whose microstructure presents equivalent fractions of austenite (γ) and ferrite (α) phases. This feature provides the material with good mechanical properties and high corrosion resistance[2,3].

Although DSSs have good mechanical properties, they are susceptible to losing corrosion resistance when they are subjected to certain thermal processes. The sensitization-related failure generated by phases' precipitation in the grain boundary region often takes place when the steel matrix presents carbon content higher than 0.03%[4]. Welding is another procedure that directly interferes with DSS microstructure; it can lead to ferritic grains' growth or disruption in the alloy's chemical composition in the heat-affected zone (HAZ)[5,6].

Variation in ferrite/austenite rates associated with the chemical composition resulting from microstructural changes in HAZ can favor the formation of intermetallic phases, mainly of those with paramagnetic features known as chi (χ) and sigma (σ) phases, which are harmful to DSS properties[7,8]. The loss of corrosion resistance properties is one of the main disadvantages of σ phase formation in DSS. According to Atamert and King[9], σ phase increase by 25% in the duplex structure can increase steel hardness by up to 80%, and it leads to a more brittle material. According to Wang et al.[10], the σ phase can act as an intermetallic deleterious phase to the duplex microstructure at concentrations higher than 1%.

The microstructural arrangement of intermetallic σ presents a ternary phase whose formation is based on high chromium content[11]. This phase's precipitation mainly takes place at the ferrite/austenite interface and it is often generated by increased chromium diffusion from the ferritic phase to the grain boundary[12-15]. Sigma phase content higher than 1% makes the material mechanically brittle and reduces its corrosion resistance[16,17]. Thus, it is essential to quantify σ phase rates close to 1% to enable both monitoring and preserving DSS quality. Accordingly, applying non-destructive techniques to surface microstructural analysis is a feasible alternative to assure quality materials in different industrial plants.

Linear sweep voltammetry (LSV) is an effective technique used to detect the σ phase in DSS[18]. Haskel et al.[19] used this technique to detect the χ and σ phases in DSS UNS S31803 presenting up to 0.9% intermetallic phases. Results in the aforementioned study which showed variations in charge density and current density, advocated for the feasibility of developing an on-site non-destructive technique assay.

Rios et al.[20] have analyzed the effect of scanning speed on peak potential (Ep) and current intensity (I) at sigma phase reactivity, based on using sweep rates (v) ranging from 1 mV s^{-1} to 10 mVs^{-1} in UNS S31803 steel samples.

*e-mail: elangabriel@ufpr.br

Tests were applied to samples with different σ phase levels ranging from 0.0% to 3.0%. LSV was conducted based on using potassium hydroxide (KOH) at 4.0 mol L^{-1} as a selective electrolyte. Based on their results, the chromium oxide film formed on the samples' surface during LSV presented a formation mechanism in compliance with the Ohmic Resistance Model[21-23] and Porous Layer Resistance Model[24].

According to Rios et al.[20], the analysis applied to the thermodynamic Ep parameter, based on using $v^{1/2}$, described the growth of a film presenting higher Cr and Mo levels associated with the σ phase content in the DSS structure. Using the thermodynamic Ep parameter enabled determining the σ phase content that does not depend on the electrode area. Thus, the analysis of results based on using charge density and current density (surface area-dependent parameter) could be replaced by the Ep assessment (surface area-nondependent parameter).

According to Haskel et al.[19], the best experimental condition for σ phase detection in DSS UNS S 31803 samples, based on using the LSV technique, was found by using 3.0 mol L^{-1} KOH solution at a scanning speed of 1.0 mV s^{-1}. However, since increased electrolyte concentration and reduced scanning speed enable better detection of the σ phase in LSV[25], the experimental design adopted by Forteski et al.[26], in association with results observed by Rios et al.[20], has shown that using 4.0 mol L^{-1} electrolyte solutions and scanning speed of 0.5 mV s^{-1} provided significant gain to this technique's sensitivity.

Based on previous research that has evidenced the importance of using non-destructive tests (NDT) to assess DSS properties, the current study aimed to investigate the correlation of sigma intermetallic phase presence to peak charge density variation and Ip and Ep parameters associated with σ phase content.

2. Methodology

The current study was carried out based on the following steps: DSS samples' cutting and tempering process, σ phase precipitation at different times of exposure to 870 °C, electrochemical surface attack, DSS microstructure phases' identification through Scanning Electron Microscopy (SEM) and Energy Dispersive Spectroscopy (EDS) analyses, and LSV tests based on using two solution-electrode working contact areas.

2.1. DSS samples' preparation

Seven UNS S-31803 stainless steel samples were previously cut, polished up to 0.1 µm alumina powder grade, and solubilized at 1100 °C, for 30 min, in a muffle furnace cooled in water at room temperature (25 °C), without agitation. This procedure was performed to establish microstructural homogeneity in DSS samples. Subsequently, six samples were subjected to different aging times (5, 10, 15, 20, 25, and 30 min) at 870 °C. One sample (called blank) was reserved as a control, for results' comparison purposes

Samples were subjected to an electrochemical surface treatment to identify DSS microstructure phases. It was done by applying 2.0 V (Minipa MPL 1305M), for 1 min, based on using graphite cathode and 1.5 mol L^{-1} potassium hydroxide (KOH) electrolyte solution (95%, NEON – CAS 1310-58-3). SEM analysis was applied to check the samples' morphology. This procedure was followed by an EDS analysis application to determine the samples' composition.

Microstructure images were reprocessed in IMAGE J™ binary counting software to quantify the contents of each sample phase. This electrochemical procedure was selected based on the KOH solution's good chemical affinity to the σ phase, and it resulted in a product with intense color[19] to be easily detected and measured.

2.2. LSV assay

Herein-performed LSV analyses were based on the microelectrode theory[19]. To do so, an electrochemical cell was assembled by following the concept of Luggin Capillary Cells. According to the electrochemical theory, Luggin-Haber capillary length and diameter affect both the volume and the ionic strength of the electrolyte at the electrode-solution interface. Luggin-Haber capillary volume is directly proportional to its length and square diameter.

Capillary volume increase can help minimize concentration gradients since it enables higher electroactive species dilution near the electrode-solution interface. However, longer capillary length can lead to longer response times due to higher ionic resistance

On the other hand, since Luggin-Haber capillary ionic resistance is directly proportional to its length and diameter, the smaller the capillary length and diameter, the lower the ionic resistance. Low ionic resistance is desirable since it minimizes the potential drop along the capillary and enables accurately measuring the electrochemical potential at the interface.

Improved LSV detection sensitivity is associated with the electrochemical cell's active internal volume since it holds the electrolyte available for electrochemical reactions to DSS. This volume refers to the contact area between the electrolyte and the DSS sample. Figure 1 shows both the dimensions and the constructive model of the electrochemical cell based on the concept of Luggin capillary. The effects of the electrolytic cell's dead volume were disregarded[27].

The electrochemical measurement instrument, known as PalmSens 2, was used to carry out voltammetry tests. This instrument is controlled by the PSTrace 4.8 electrochemical

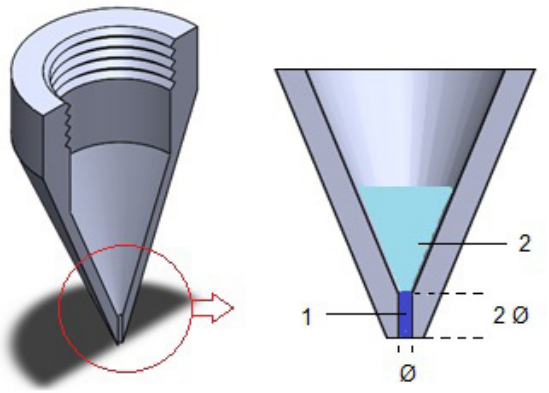

Figure 1. Constructive model of the electrochemical cell based on the concept of Luggin capillary, wherein: 1 – Reaction's active volume, 2 - Dead volume.

interface software. DSS samples were previously subjected to surface finishing by sanding (3M – P 600) to standardize the analyses. According to Haskel et al.[19], samples were subjected to the electrochemical pickling step at the beginning of the experiments to rule out any external interference with the working electrode surface. It was done by applying the electric potential of -0.1 V, for 8 s. LSVs were conducted based on the methodology of three electrodes, namely: the working electrode (UNS S-31803 sample), the counter-electrode (platinum – Pt) and the saturated calomel reference electrode (Analyzer – 3A41-FH). The experimental apparatus used in the trials is shown in Figure 2.

Because increased electrolyte concentration and reduced scanning speed enable better detecting the σ phase in LSV, the experimental conditions adopted for analysis purposes comprised: electrolyte concentration of 4.0 mol L^{-1} of KOH (90.7%, Reatec – CAS 1310-58-3) used as electrolyte solution, complexed with 0.1 mol L^{-1} of KCL (99.43%, Neon – CAS 7447-40-7) and 0.01 mol L^{-1} of Ethylene Glycol (99.8%, Alphatec – CAS 107-21-1) termed as Standard Solution[1]. Two solution-electrode contact-working areas of each sample - 0.3318 mm^2 and 0.7854 mm^2 - were analyzed at a scan rate of 0.5 mV s^{-1}. Trials were performed in duplicate.

2.3. Samples' analysis and quantifications

Peak current (Ip) values were obtained from the resulting LSV voltammograms and current density (Jp) was calculated by taking into consideration the electrolyte-electrode area (A) exposure, based on Equation 1:

$$Jp = Ip / A \quad (1)$$

The charge (Q) resulting from the electrochemical reaction was also found by taking into account the peak current and the time (t) required for this peak to take place, based on Equation 2:

$$Q = \int Ip\, dt \quad (2)$$

3. Results and Discussions

Table 1 presents chemical composition values observed for the control DSS sample (blank).

It was possible to see that the control sample presented typical DSS UNS S31803 composition by comparing these results to contents set by the standard established for ASTM A 276-02a stainless steels[28].

3.1. Samples' analysis and quantification

The electrochemical technique based on KOH alkaline solution is a good alternative among several DSS phase quantification methods adopted to enhance σ phase features through electric potential action[29].

SEM micrographs taken from samples subjected to different aging times are shown in Figure 3. This analysis enabled the detecting of the σ phase with a black hue, the ferritic phase with a dark gray color, and the austenitic phase with a light gray shade. It is worth mentioning that SEM is a high-resolution technique used in electron microscopy. In addition, it provides significant magnification, at a highly detailed level, besides enabling the obtainment of fundamental information about the investigated materials' structure and properties.

Two features were observed in the elements found in the σ and χ intermetallic phases of the UNS S31803 steel based on Figure 3: Cr and Mo segregation to the grain contour, which led to these elements' dispersion; and to the formation of a thicker oxide film in the intermetallic phase region due to higher electrolyte reactivity to increased Cr levels, which turns the σ or χ phase staining darker.

Identifying the black staining points in the micrograph, as a process associated with the σ phase exposed in the microstructure, meant analyzing the count of elements, such as Cr, whose concentration decreases when it is transformed from ferritic grain into intermetallic phase. The sample aged at 870°C, for 30 minutes, which presented the highest phase transformation kinetics, had its surface analyzed via EDS to determine changes in the presence of elements typical of each phase.

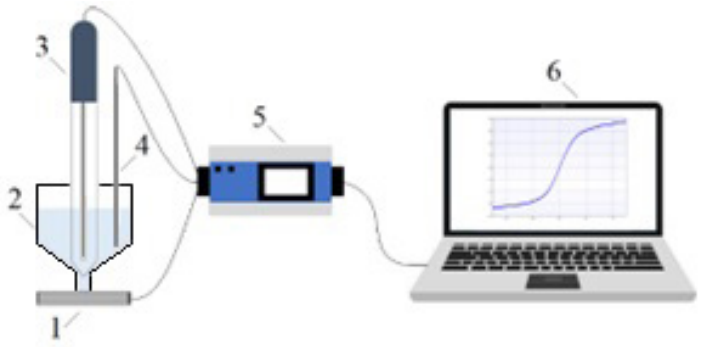

Figure 2. Experimental apparatus used in LSVs, comprising: 1 - working electrode (DSS sample), 2 - electrolyte cell, 3 - calomel reference electrode, 4 - counter-electrode (Pt), 5 - electrochemical interface (Palm Sens 2) and 6 - computer for data acquisition purposes.

Table 1. Chemical composition of the analyzed UNS S31803 steel.

Element	C	Cu	Cr	Fe	Mo	Mn	Ni	P	S	Si
Concentration (%)	1.93	0.07	21.99	65.70	2.76	1.05	6.03	0.00	0.15	0.32

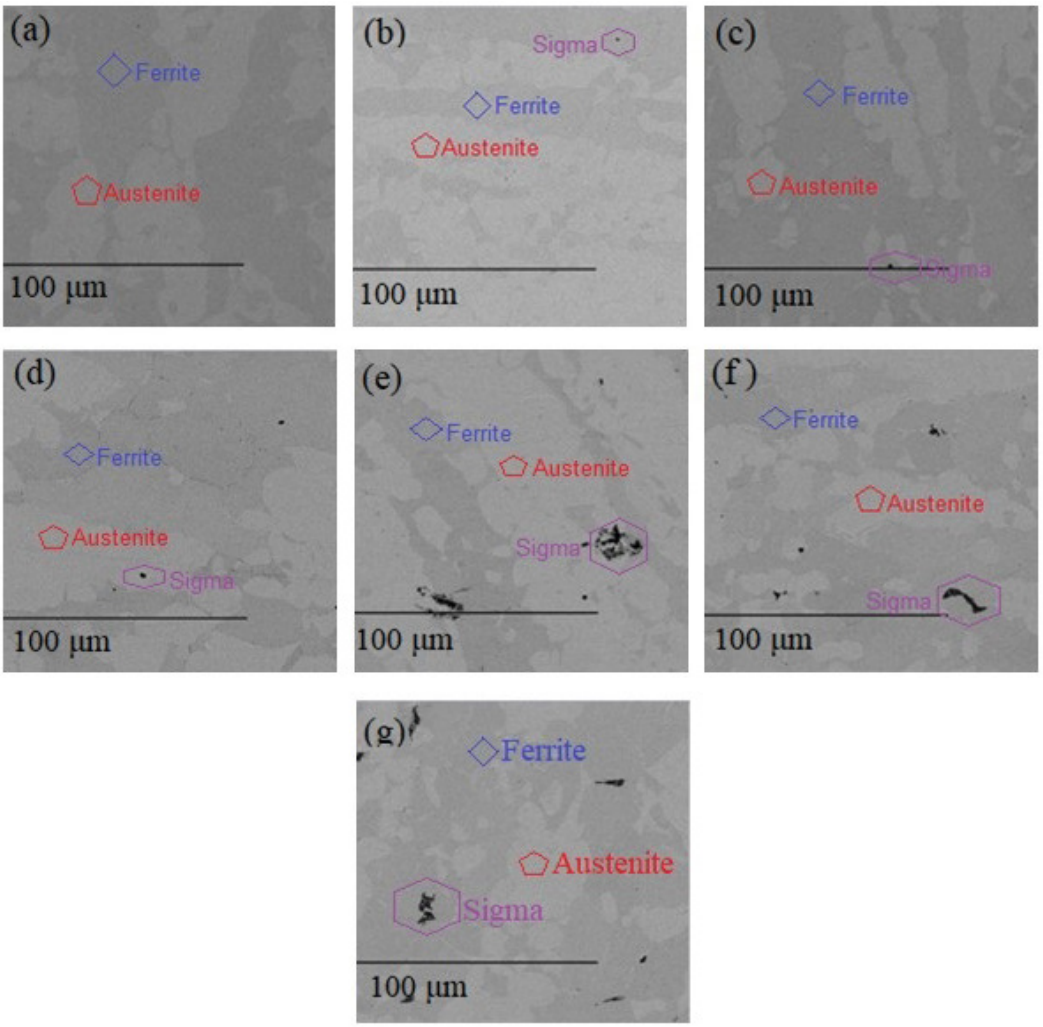

Figure 3. SEM micrograph taken from samples subjected to different aging times at 870 °C: (a) Blank, (b) 5-minute aging, (c) 10-minute aging, (d) 15-minute aging, (e) 20-minute aging, (f) 25-minute aging, and (g) 30-minute aging.

The high intermetallic phase concentration observed in the sample aged for 60 minutes has evidenced that the feature of the oxide formed in this area was associated with the kinetics of the selective reaction mechanism of the KOH solution's electrolytic attack at the σ phase. The distribution map plotted for elements found in each UNS S31803 steel phase, based on EDS, is shown in Figure 4.

The analysis of phases' elemental composition, based on the EDS technique, identified the sigma intermetallic phase associated with segregation elements involved in (Fe-Cr-Mo) phase formation. In addition, the greater-thickness oxide-film formation over the intermetallic phases was related to the selective reactive phenomenon presented by the potassium hydroxide electrolyte (KOH), which interacts with hydroxide chromium formation in the σ phase[30].

The amount of intermetallic σ phase was calculated through image processing in the IMAGE JTM software. The results of this quantification are shown in Table 2.

Based on Table 2, longer aging exposure time has contributed to σ phase formation.

Table 2. σ phase rate per unit area.

Sample	Aging time (min)	σ phase (%)
1*	0	0.000
2	5	0.040
3	10	0.310
4	15	0.440
5	20	0.876
6	25	1.142
7	30	1.693

*Control - blank sample.

3.2. LSV analysis

Samples were subjected to voltammetry analysis after determining the σ phase content of each aging time. Voltammetry was conducted in duplicate and it included the control (σ phase-free) sample, which was used to compare LSV results observed for other samples.

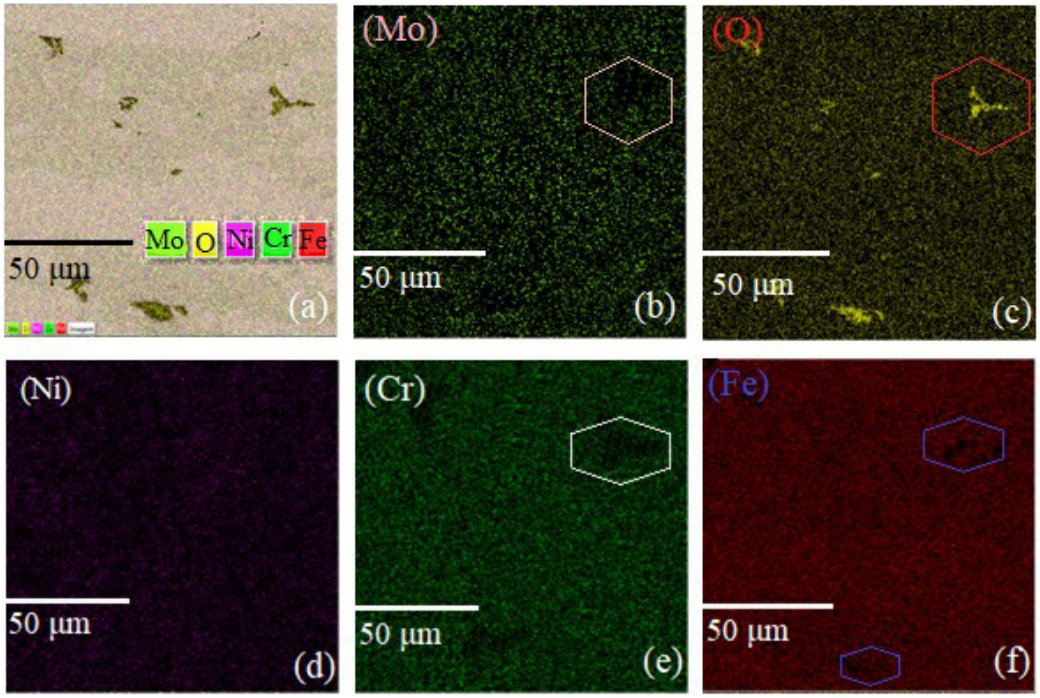

Figure 4. Distribution map plotted for elements found in each phase of 60-minute aged UNS S31803 steel, with a view of the transformation mechanism of phases observed in the presence of intermetallic sigma. Namely: (a) General map, (b) presence of Molybdenum, (c) presence of Oxygen, (d) presence of Nickel, (e) presence of Chromium, (f) presence of Iron.

Voltammograms shown in Figure 5a to g represent the voltammetric runs performed for each aging range, according to which, blue (Run1) and red (Run 2) curves represent the duplicate of the test performed with the smallest electrochemical attack area (0.3318 mm^2), whereas orange (Run 3) and green (Run 4) curves represent the duplicates performed in the test conducted with the largest electrochemical attack area (0.7854 mm^2). Voltammetry was conducted by following the adopted standard based on using the same sample position in all scanning procedures. This approach aimed at reducing potential error and variation sources in the electrochemical properties throughout the intermetallic concentration range of the analyzed samples. Moreover, it enabled finding accurate results for the calculation of current densities in all tests.

Current and potential peaks determined for analysis purposes are shown in Figure 6. There was variation in Ip and Ep parameters as the intermetallic phase concentration increased. Run 3 and Run 4 duplicates (in blue) represent the electrochemical peak of the control sample (Blank), whereas Run 3 and; Run 4 (in yellow) represent the electrochemical peak of sample 7 with 1.6934% σ phase. This finding indicates the peak shift to more reactive electrochemical potential ranges and increase in current, based on the same measurement parameters.

Figure 7 shows Ip behavior over aging time, based on peak current (Ip) values, by using electrolyte-electrode contact area of 0.7854 mm^2.

Overall, the increase observed in samples' intermetallic concentration favored peak current increase. However, samples 2 and 3 (Table 2), which presented σ phase concentrations up to 0.31%, did not present significant changes in Ip values in comparison to the control sample. Thus, the LSV technique did not show sensitivity in detecting σ phase levels below this concentration, under this condition.

The microelectrodes concept-based use of electrochemical cells is associated with the process of measuring small reaction potentials, and it helps improve the sensitivity of the current (I) / potential (E) electrochemical interaction mechanism in small reaction areas[24]. In addition, according to the Luggin capillary model, using microelectrodes favors oxide film formation through the ohmic resistance model[23], as well as porous layer film formation[31]. Both herein-described reaction mechanisms were confirmed by Rios et al.[20], who assessed the correlation of σ phase content to Ep and Ip in chromium oxide film formation in UNS S-31803 samples.

Voltammetric scanning procedures were performed in areas beyond the 0.7854 mm^2 electrode to check how a smaller reaction area (0.3318 mm^2) could affect the detection capacity of current and potential peak parameters. It was done to establish the association of intermetallic phases with the effect of the electrochemical interaction area of the microelectrode in LSV assays. The current profile presenting samples' different aging times, for the smallest electrochemical reaction area is shown in Figure 8.

Results presented in Figure 8 did not show significant variations in Ip values. This behavior indicates low sensitivity to detect the analyzed intermetallic level. This result does not meet previous results observed for microelectrodes, based on the Luggin capillary concept

Charge density (Q) values were calculated by taking into consideration both areas in Figure 7 and Figure 8 to help understand the effect of microelectrode area reduction on

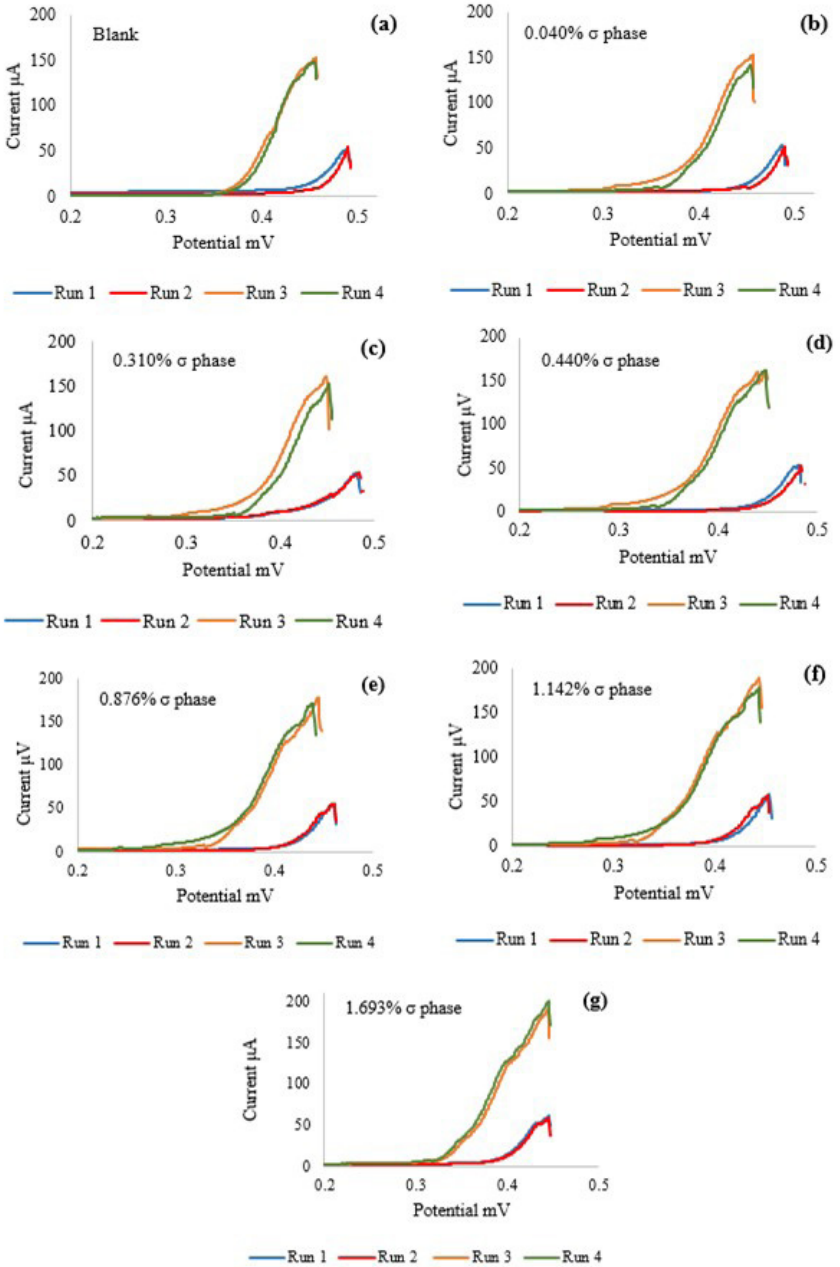

Figure 5. Voltammogram performed based on using Standard Solution (1) and scanning speed fixed at 0.5mV s^{-1}. Curves 1 and 2 were performed based on using an attack area of 0.3318 mm^2, whereas curves 3 and 4 were performed based on an attack area of 0.7854 mm^2. Samples comprised (a) blank (b) sample 2 (0.04% σ phase), (c) sample 3 (0.310% σ phase), (d) sample 4 (0.440% σ phase), (e) sample 5 (0.876% σ phase), (f) sample 6 (1.1420% σ phase), and (g) sample 7 (1.693% σ phase).

LSV results. Electrochemical reactions' charge density was associated with chromium oxide film formation on the DSS surface[20], based on peak current formation time.

This analysis was performed to check the correlation of intermetallic phase concentration to charge density variation (ΔQ). ΔQ values were calculated by subtracting the mean charge density value observed for the control sample from that of samples presenting the σ phase ($\Delta Q = Q_{sample} - Q_{blank}$). Figure 9 shows the ΔQ behavior of samples correlated with different electrolyte-electrode contact areas.

Variation in ΔQ values recorded for different intermetallic σ phase concentrations, with the performance for each surface area, suggested that using the microelectrode concept has positively influenced variations in ΔQ values and improved the investigated technique's sensitivity.

LSV assays performed with the electrode presenting an area of 0.3318 mm^2 recorded the highest ΔQ values (Figure 9). Sample 5 (0.876% of σ phase), which presents σ phase concentration close to the critical content of the intermetallic phase (1%), recorded charge variation of 2.7 C

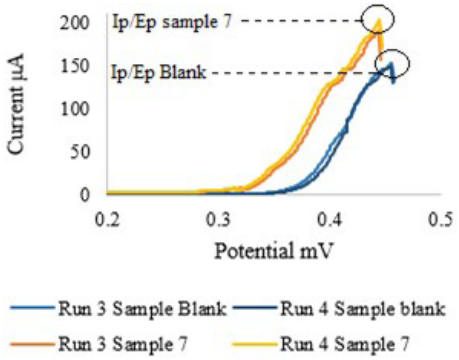

Figure 6. Voltammogram depicting changes in Ip and Ep as the σ phase increased. It was performed based on using Standard Solution (1) and scanning speed fixed at 0.5mV s^{-1}. Curves 1 and 2 were used as blank samples, whereas curves 3 and 4 represented sample 7 (1.6934% σ phase). Voltammogram was conducted based on using attack area of 0.7854 mm^2.

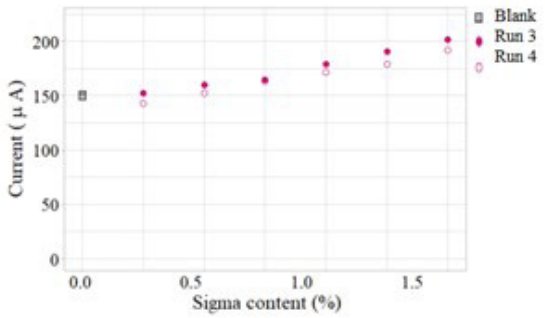

Figure 7. Current obtained based on using an exposure area of 0.7854 mm^2.

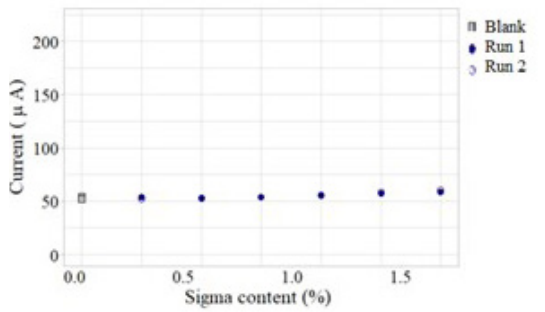

Figure 8. Current obtained based on using an exposure area of 0.3318 mm^2.

for the electrode with an area of 0.7854 mm^2. On the other hand, the same sample presented a charge variation of 44 C when the electrode with an exposure area of 0.3318 mm^2 was used. As for Sample 2 (0.04% of σ phase), the larger electrode area recorded change at the order of 0.6 C, whereas the reduced-area electrode presented a charge variation of 7.0 C.

The analysis of ΔQ results enabled assessing the electrochemical assay accuracy and sensitivity under different

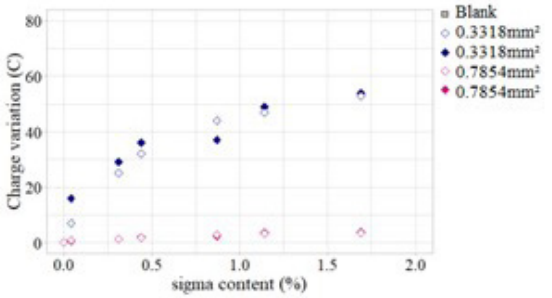

Figure 9. Charge variation in samples based on sigma content and on two contact areas.

experimental conditions. These results are essential to help optimize the electrochemical tests and develop new surface analysis methodologies.

The reaction potential (E) of a given material is linked to variations in the Gibbs free energy (ΔG), wherein ΔG = -nFE, n is the number of electrons involved in the reaction and F is the Faraday constant (96,450 C mol^{-1}). Based on Figure 3, the surface area of DSS samples presented both the γ and α phases, as well as the grain interface or contour (gc) region, and the intermetallic σ phase, which has low stability and is considered a metastable phase. The ΔG stability order observed for the investigated regions is given by: ΔGσ < ΔGgc < ΔGα < ΔGγ. Therefore, the higher the intermetallic phase volume found in the steel microstructure, the lower its stability during electrochemical reactions. Therefore, chromium oxide formation will take place at lower potentials in comparison to the control sample.

Figure 10 and Figure 11 show variations in Ip and Ep parameters based on the σ phase content observed for the two assessed electrolyte/electrode contact areas. Based on the herein performed analyses, the Ip value increased as the σ phase content increased. Increased intermetallic concentration also resulted in Ep displacement to the most negative values. In addition, using the electrode presenting the smallest reaction area (0.3318 mm^2) has contributed to increasing the investigated technique's detection sensitivity, besides evidencing higher consistency in Ep parameters' results due to σ phase increase.

The electrode surface area of 0.7854 mm^2 presented higher Ep dispersion and lower Ep change at different intermetallic phase levels. Thus, the analysis applied to the Ep effect based on σ phase content did not show significant LSV sensitivity. Only changes in Ip values recorded for the analyzed area were considered significant.

Based on the analysis applied to the smallest electrochemical reaction area (0.3318 mm^2), Ip and Ep parameters presented lower dispersion and greater linearity according to the variation in intermetallic phase content. Thus, it is possible to state that using the smallest electrode area increased the LSV technique sensitivity to detect the σ phase in comparison to the largest electrode area.

Using a smaller reaction area enabled finding a closer correlation of Ip and Ep parameters to intermetallic phase incidence. Data deriving from the voltammogram performed in LSV enabled higher sensitivity to detect the σ phase, as

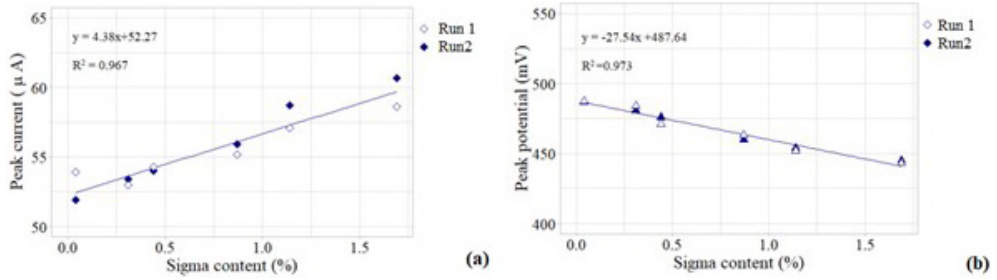

Figure 10. Peak current - Ip (a) and peak potential - Ep (b) obtained from LSV electrode surface area = 0.3318 mm^2.

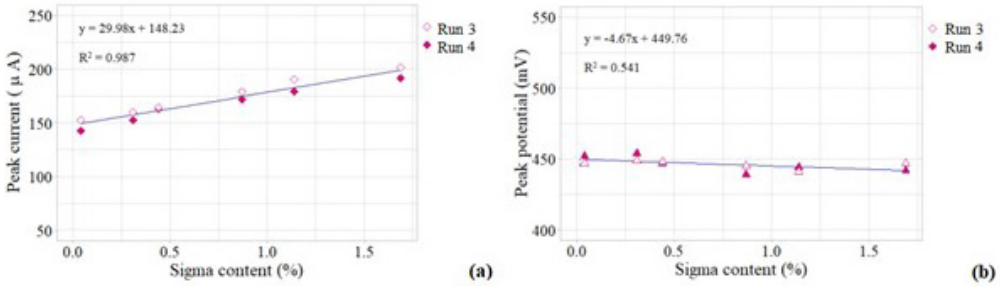

Figure 11. Peak current - Ip (a) and peak potential - Ep (b) obtained from LSV electrode surface area = 0.7854 mm^2.

well as direct Ip and Ep correlation to σ phase concentration close to 0.04%.

These findings have evidenced the importance of using the LSV technique to both analyze and detect intermetallic phases in DSS. Using a reduced reaction area, in compliance with the microelectrodes concept, helps increase the sensitivity of this technique and enables accurately correlating charge peak current and potential parameters to the intermetallic phase level.

4. Conclusion

The present study assessed the effect of electrolyte-electrode exposure area, based on the microelectrodes concept, on improving LSV technique sensitivity to detect the σ phase concentration in DSS. To do so, different LSV assays were conducted based on using electrolyte concentration (KOH) of 4 mol L^{-1} and a scanning speed of 0.5 V s^{-1}. The voltammetry assay presenting the highest charge density variation (ΔQ) was conducted with the electrolyte-electrode contact area of 0.3318 mm^2, which corresponded to the smallest exposure area and led to a variation of 44 C, whereas the largest reaction area led to charge density variation of 2.7 C. Since the current charge is associated with chromium oxide film formation on the DSS surface, reducing the electrode exposure area favors this oxidation reaction and increases the reaction charge (Q), which, in turn, contributes to increasing the σ phase-detection sensitivity via LSV. The improved sensitivity of this technique enabled correlating lower dispersion and higher linearity to the intermetallic phase content associated with variations in Ip and Ep parameters. Thus, the incidence ratio observed for Ip (at 52 µA) and Ep (at 490 mV) in sample 1, without intermetallic phase incidence, as well as for Ip (at 60 µA) and Ep (at 443 mV) in sample 7, with 1.69% σ phase, was calculated. Both results were recorded for the electrode with the smallest reaction area. Thus, results related to σ phase detection through LSV assay can be directly associated with variations in Ip and Ep parameters due to increased intermetallic phase concentration. This finding established a breakthrough in surface technique-detection sensitivity.

5. Acknowledgement

The authors are grateful to CAPES (Coordenação de Aperfeiçoamento de Pessoal de Nível Superior – Brasil – Finance Code 001), for the financial support provided to this research, as well as to the Electron Microscopy Center of Federal University of Paraná and the Human Resources Program of the National Agency for Petroleum, Natural Gas and Biofuels (PRH-ANP), for the support provided with resources deriving from the investment of oil companies qualified in the P, D&I Clause of ANP Resolution N. 50/2015).

6. References

1. Llorca-Isern N, Biserova-Tahchieva A, Lopez-Jimenez I, Calliari I, Cabrera JM, Roca A. Influence of severe plastic deformation in phase transformation of superduplex stainless steels. J Mater Sci. 2019;54(3):2648-57. http://doi.org/10.1007/s10853-018-2984-y.
2. Donik Č, Kocijan A, Grant JT, Jenko M, Drenik A, Pihlar B. XPS study of duplex stainless steel oxidized by oxygen atoms. Corros Sci. 2009;51(4):827-32. http://doi.org/10.1016/j.corsci.2009.01.021.

3. Swens JJ, Kolster BH. σ- Phase precipitation in a duplex stainless steel: an APFIM investigation. Surf Sci. 1991;246(1-3):252-9. http://doi.org/10.1016/0039-6028(91)90423-P.
4. Zheng C, Wang G, Wu X, Ai Z. Failure analysis of duplex stainless steel in an atmospheric tower. In: ASME 2018 Pressure Vessels and Piping Conference; 2018; Prague, Czech Republic. Proceedings. New York: American Society of Mechanical Engineers; 2018. (vol. 5). http://doi.org/10.1115/PVP2018-84348.
5. Zhang Z, Jing H, Xu L, Han Y, Zhao L. Investigation on microstructure evolution and properties of duplex stainless steel joint multi-pass welded by using different methods. Mater Des. 2016;109:670-85. http://doi.org/10.1016/j.matdes.2016.07.110.
6. Higelin A, Le Manchet S, Passot G, Cissé S, Grocki J. Heat-affected zone ferrite content control of a duplex stainless steel grade to enhance weldability. Weld World. 2022;66(8):1503-19. http://doi.org/10.1007/s40194-022-01326-0.
7. Biezma MV, Martin U, Linhardt P, Ress J, Rodríguez C, Bastidas DM. Non-destructive techniques for the detection of sigma phase in duplex stainless steel: a comprehensive review. Eng Fail Anal. 2021;122:105227. http://doi.org/10.1016/j.engfailanal.2021.105227.
8. Olsson C-OA, Landolt D. Passive films on stainless steels: chemistry, structure and growth. Electrochim Acta. 2003;48(9):1093-104. http://doi.org/10.1016/S0013-4686(02)00841-1.
9. Atamert S, King JE. Sigma-phase formation and its prevention in duplex stainless steels. J Mater Sci Lett. 1993;12(14):1144-7. http://doi.org/10.1007/BF00420548.
10. Wang R, Imagawa M, Honda M, Fukuhara H. Single loop electrochemical potentiokinetic reactivation behaviour of continuously cooled SUS329J4L duplex stainless steel. Int J Mech Syst Eng. 2017;3(1). http://doi.org/10.15344/2455-7412/2017/125.
11. Connor LD, Mignanelli PM, Christofidou KA, Jones NG, Baker AR, Tang CC, et al. *In situ* study of sigma phase formation in Cr–Co–Ni ternary alloys at 800 °C using the long duration experiment facility at Diamond Light Source. J Synchrotron Radiat. 2018;25(5):1371-8. http://doi.org/10.1107/S1600577518009475.
12. Pohl M, Storz O, Glogowski T. Effect of intermetallic precipitations on the properties of duplex stainless steel. Mater Charact. 2007;58(1):65-71. http://doi.org/10.1016/j.matchar.2006.03.015.
13. Warren AD, Harniman RL, Guo Z, Younes CM, Flewitt PEJ, Scott TB. Quantification of sigma-phase evolution in thermally aged 2205 duplex stainless steel. J Mater Sci. 2016;51(2):694-707. http://doi.org/10.1007/s10853-015-9131-9.
14. Melo EA, Magnabosco R. Influence of the heterogeneous nucleation sites on the kinetics of intermetallic phase formation in aged duplex stainless steel. Metall Mater Trans, A Phys Metall Mater Sci. 2017;48(11):5273-84. http://doi.org/10.1007/s11661-017-4299-z.
15. Elsaady MA, Khalifa W, Nabil MA, El-Mahallawi IS. Effect of prolonged temperature exposure on pitting corrosion of duplex stainless steel weld joints. Ain Shams Eng J. 2018;9(4):1407-15. http://doi.org/10.1016/j.asej.2016.09.001.
16. Deng B, Wang Z, Jiang Y, Wang H, Gao J, Li J. Evaluation of localized corrosion in duplex stainless steel aged at 850 °C with critical pitting temperature measurement. Electrochim Acta. 2009;54(10):2790-4. http://doi.org/10.1016/j.electacta.2008.11.038.
17. Souza DDBG, Vilarinho LO. Influence of present phases in corrosion and mechanical behavior of UNS S31803 duplex stainless steel welded by conventional short circuit MIG/MAG process. J Mater Res Technol. 2020;9(5):11244-54. http://doi.org/10.1016/j.jmrt.2020.08.026.
18. Sampaio MTG, Furtado AB, Ignácio MDC, Tavares SSM, Pardal JM, Pimenta AR, et al. DL-EPR vs. LSV-KOH: from simple detection of deleterious phases to analysis of morphology and high accuracy on determination of sigma phase in UNS S32750 stainless steel. Corros Eng Sci Technol. 2023;58(1):1-11. http://doi.org/10.1080/1478422X.2022.2128376.
19. Haskel HL, Sanches LS, Ponte HA. A new methodology of nondestructive testing for quantitative evaluation of sigma phase in duplex stainless steels. Mater Res. 2019;22(3):e20180682. http://doi.org/10.1590/1980-5373-mr-2018-0682.
20. Rios JO, Forteski EG, Ponte MJJS, Ponte HA. Evaluation of voltametric profiles for quantitative estimation of sigma phase (σ) content in duplex stainless steel UNS S31803: an ohmic and layers porous resistance models (LPRM) analysis. Braz J Dev. 2023;9(2):7032-44. http://doi.org/10.34117/bjdv9n2-060.
21. D'Alkaine CV, Cordeiro JMM. Active-passive transition of lead in sulfuric acid solutions. In: Bullock KR, Pavlov D, editors. Advances in lead acid batteries. Pennigton: Electrochemical Society; 1984. (vol. 1).
22. D'Alkaine CV, de Souza LMM, Nart FC. The anodic behaviour of niobium—III. Kinetics of anodic film growth by potentiodynamic and galvanostatic techniques—general models, equations and their applications. Corros Sci. 1993;34(1):129-49. http://doi.org/10.1016/0010-938X(93)90264-H.
23. D'Alkaine CV, Tulio PC, Berton MAC. Quantitative Ohmic model for transient growths of passivating films. Electrochim Acta. 2004;49(12):1989-97. http://doi.org/10.1016/j.electacta.2003.12.029.
24. Calandra AJ, Tacconi NR, Pereiro R, Arvia AJ. Potentiodynamic current/potential relations for film formation under OHMIC resistance control. Electrochim Acta. 1974;19(12):901-5. http://doi.org/10.1016/0013-4686(74)85041-3.
25. Sampaio MTG, Furtado AB, Tavares SSM, Pardal JM, Macêdo MCS, Velasco JAC, et al. Sigma and chi phases analysis in UNS S32750 superduplex stainless steel by optimized linear sweep voltammetry in alkaline medium. J Electrochem Soc. 2020;167(10):101507. http://doi.org/10.1149/1945-7111/ab9b0e.
26. Forteski EG, Pires CMG, Ponte HA, Ponte MJJS. Application of linear sweep voltammetry for detection of low sigma phase contents in duplex stainless steel. In: Congresso Internacional de Engenharia Mecânica e Industrial; 2021; Belo Horizonte, MG. Proceedings. Recife: Even3; 2021.
27. Bard AJ, Faulkner LR. Electrochemical methods: fundamentals and applications. 1st ed. New York: Wiley; 1983. (vol. 20).
28. ASTM: American Society for Testing and Materials. ASTM A276-13a: standard specification for stainless steel bars and shapes. West Conshohocken: ASTM; 2023.
29. Chan K, Tjong S. Effect of secondary phase precipitation on the corrosion behavior of duplex stainless steels. Materials. 2014;7(7):5268-304. http://doi.org/10.3390/ma7075268.
30. Yao J, Macdonald DD, Dong C. Passive film on 2205 duplex stainless steel studied by photo-electrochemistry and ARXPS methods. Corros Sci. 2019;146:221-32. http://doi.org/10.1016/j.corsci.2018.10.020.
31. Brunetti V, Villullas HM, López Teijelo M. Potentiodynamic growth of anodic silver chromate layers. Electrochim Acta. 1999;44(26):4693-700. http://doi.org/10.1016/S0013-4686(99)00220-0.